J. Mech. Phys. Solids 178 (2023) 105359

Contents lists available at ScienceDirect

Journal of the Mechanics and Physics of Solids

journal homepage: www.elsevier.com/locate/jmps

Atomistic determination of Peierls barriers of dislocation glide in nickel

Yipin Si [a], Yin Zhang [a], Dengke Chen [a], Jonathan L. Wormald [b], Benjamin S. Anglin [b], David L. McDowell [a], Ting Zhu [a,*]

[a] Woodruff School of Mechanical Engineering, Georgia Institute of Technology, Atlanta, GA 30332, USA
[b] Naval Nuclear Laboratory, West Mifflin, PA 15122, USA

ARTICLE INFO

Keywords:
Peierls barrier
Atomistic modeling
Nudged elastic band method
Face-centered cubic metal

ABSTRACT

The Peierls barrier measures the lattice resistance to dislocation glide in crystalline solids. We use the nudged elastic band (NEB) method to calculate the Peierls barriers for screw and edge dislocation glide in a face-centered cubic (FCC) metal of Ni. The minimum energy paths (MEPs) across single or sequential Peierls barriers are determined under shear loading. The NEB results show the decreasing Peierls barrier with increasing shear stress, giving the Peierls stress at which the Peierls barrier vanishes. The effects of boundary condition and system size on Peierls barriers are studied by comparing strain- and stress-controlled NEB results. Furthermore, the free-end NEB methods are applied to determine MEPs with improved computational efficiency. The NEB results are also used to evaluate the energetic driving force of dislocation glide, which is consistent with that determined from the Peach-Koehler force. The accuracy of the present NEB results based on an empirical interatomic potential is assessed by comparison with a machine-learning potential. This work demonstrates the robust and efficient quantification of Peierls barriers to dislocation glide in an FCC metal, and it lays a solid foundation for the atomistic determination of Peierls barriers in compositionally complex alloys with the FCC structure in future studies.

1. Introduction

Dislocation glide plays an important role in plastic deformation of crystalline solids. The lattice resistance to dislocation glide is usually characterized by the Peierls (1940) barrier. Early work by Cottrell (1953), Nabarro (1947), Peierls (1940) estimated the dislocation energy per unit length as a function of dislocation position without applied loading, and showed that it oscillates due to the periodic structure of the crystal lattice. The maximum energy is termed the Peierls barrier. An applied shear stress on the dislocation glide plane serves to reduce the Peierls barrier. The critical resolved shear stress for dislocation glide when the Peierls barrier is reduced to zero is called the Peierls stress. Extensive theoretical and experimental estimates have been given for the Peierls barrier and Peierls stress in the literature (Nabarro, 1997; Schoeck, 1999; Szelestey et al., 2003).

Recent studies of dislocation glide resistances in compositionally complex alloys (Ding et al., 2019; George et al., 2020; Li et al., 2019; Ren et al., 2022) have rekindled interest in the quantitative determination of Peierls barriers in face-centered cubic (FCC) metals and alloys. Accurate quantification of the Peierls barriers in unary FCC metals is a necessary first step toward further study of more

* Corresponding author.
E-mail address: ting.zhu@me.gatech.edu (T. Zhu).

https://doi.org/10.1016/j.jmps.2023.105359
Received 26 November 2022; Received in revised form 11 May 2023; Accepted 8 June 2023
Available online 11 June 2023

compositionally complex FCC alloys. Atomistic simulations such as molecular statics and molecular dynamics (MD) have been applied to study Peierls barriers in FCC metals (Bulatov et al., 1999; Lu et al., 2000; Shin and Carter, 2013; Wang et al., 2011). However, use of molecular statics in energy minimization is only suitable to determine the Peierls stress at which the stress-dependent Peierls barrier vanishes. In contrast, MD can be applied to calculate stress-dependent Peierls barriers. However, MD is limited to high dislocation velocities due to its timescale limitation (Li et al., 2019). In addition, coarse-grained models are used to evaluate Peierls barriers based on the periodic relation of shear stress versus slide displacement across the slip plane (Nabarro, 1997; Schoeck, 1999; Szelestey et al., 2003). However, atomic bonding interactions at the dislocation core can be overly simplified in those models, affecting the accuracy of Peierls barriers. Hence, there is currently a lack of systematic full-atomistic studies of Peierls barriers in FCC metals as a function of applied stress (Cai et al., 2004).

The nudged elastic band (NEB) method (Jonsson et al., 1998; Zhu et al., 2013) enables an effective atomistic determination of the Peierls barrier as a function of applied loading. Based on transition state theory (Phillips, 2001; Vineyard, 1957), the rate of dislocation glide from a Peierls valley to a neighboring one in a crystal lattice is given by

$$v = v_0 \exp\left(-\frac{\Delta G(\tau, T)}{k_B T}\right) \tag{1}$$

where v_0 is the trial frequency, ΔG is the activation Gibbs free energy, τ is the applied resolved shear stress on the dislocation slip system, T is the temperature, and k_B is the Boltzmann constant. Based on harmonic transition state theory (Phillips, 2001; Vineyard, 1957), the temperature effect on ΔG in Eq. (1) can be incorporated into the prefactor v_0. Hence, one can focus on the temperature-independent part of ΔG, which is the activation Gibbs free energy at 0 K. This activation energy can be calculated from the Gibbs free energy surface of an atomic system at 0 K using the stress-controlled NEB method, and it is referred to as the Peierls barrier in this work. Similarly, when the load is applied by a shear strain γ instead of a shear stress τ, $\Delta G(\tau, T)$ in Eq. (1) should be replaced by the activation Helmholtz free energy $\Delta F(\gamma, T)$. Correspondingly, one can focus on the temperature-independent part of ΔF, which is the activation Helmholtz free energy at 0 K. This activation energy can be calculated from the Helmholtz free energy surface of an atomic system at 0 K using the strain-controlled NEB method, and it is also referred to as the Peierls barrier in this work.

The NEB method has been used to study the Peierls barriers of dislocation glide in body-centered cubic (Bai and Fan, 2018; Narayanan et al., 2014; Rodney and Proville, 2009; Rodney et al., 2017; Wang et al., 2022) and hexagonal close-packed (Wu and Curtin, 2015) metals, and some other phenomena like phase transformation in silicon (Ghasemi et al., 2019). However, there are few reports on the NEB studies of Peierls barriers in FCC metals in the literature (Rodney and Proville, 2009; Shin and Carter, 2013). This is largely because these Peierls barriers are usually low and the corresponding NEB calculation requires some attention to delicate control of dislocation structure and applied loading (Chen et al., 2019; Zhang et al., 2022).

In this work, we achieve the robust and efficient application of the NEB method for calculating the Peierls barriers in a representative FCC single crystal of Ni. We apply both the strain-controlled and stress-controlled NEB methods to reveal the effects of boundary condition and system size. We also apply the stress-controlled free-end NEB method (Zhu et al., 2007, 2008) for improving computational efficiency. Furthermore, we use the Peach-Koehler force (Peach and Koehler, 1950) to validate the atomistically calculated energy decrease for a dislocation moving from a Peierls valley to a neighboring one under an applied shear stress. All the NEB calculations are performed using LAMMPS (Thompson et al., 2022), and a representative script for the stress-controlled NEB calculation can be obtained by contacting the corresponding author of this paper to facilitate the verification and extension of our results by other research groups. This work lays a solid foundation for the atomistic determination of Peierls barriers in

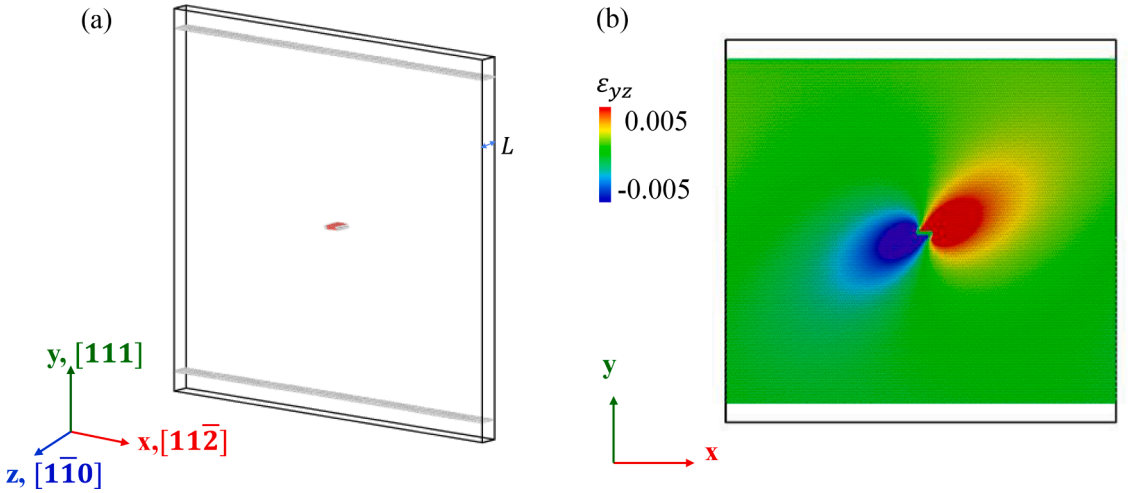

Fig. 1. NEB simulation setup of a ½[1$\bar{1}$0](111) screw dislocation. (a) An FCC Ni slab containing a screw dislocation. Atoms in the perfect FCC structure are removed for displaying atoms at the dislocation core and surface. (b) Contour of shear strain ε_{yz} in the slab. All the atomic configurations in this paper are displayed using the atomic structure visualization tool OVITO (Stukowski, 2010).

compositionally complex alloys with the FCC structure in the future.

2. Peierls barrier of screw dislocation glide without applied loading

The NEB method is an efficient chain-of-states approach for finding the minimum energy path (MEP) between a given initial and final state of a transition on the potential energy surface of an all-atom system (Jonsson et al., 1998; Zhu et al., 2013). The initial and final states are two local minima on the potential energy surface. In a conventional NEB calculation, the initial and final states are first obtained by the conjugate gradient method for energy minimization. Then a set of images (termed replicas) along an initial elastic band is constructed between the initial and final states. The elastic band is relaxed to obtain an MEP and associated saddle point(s) between the initial and final states. When a single saddle point is obtained along an MEP, the energy barrier is the energy difference between the saddle-point and initial states. When multiple saddle points are obtained, the energy barrier associated with a saddle point is the energy difference between the saddle point and the proceeding local minimum along the MEP.

To calculate the energy barrier, i.e., Peierls barrier, of glide of a $\frac{1}{2}[1\bar{1}0](111)$ screw dislocation in Ni, we set up a rectangular FCC Ni slab in a supercell, as shown in Fig. 1a. The slab has the size of 40 × 40 × 2 nm in the x//$[11\bar{2}]$, y//[111], and z//$[1\bar{1}0]$ directions, respectively. We use a small slab thickness along the z-direction to study the two-dimensional mode of dislocation glide. Namely, the dislocation line in each replica along the MEP remains straight, such that the Peierls barrier is given as eV per unit length along the z direction. For each NEB calculation without applied loading, the top and bottom y-surfaces of the slab are traction free, while periodic boundary conditions are imposed along the x and z directions. The embedded atom method (EAM) potential by Angelo et al. (1995) is used to represent the interatomic interaction between Ni atoms. A straight screw dislocation line is embedded into the middle of the slab by first imposing a displacement field to all atoms according to the elastic solution of a screw dislocation and then relaxing the slab with the conjugate gradient method for energy minimization. The resulting atomic configuration in Fig. 1a corresponds to a local energy minimum state, and it contains a single screw dislocation that dissociates into two Shockley partials with a stacking fault ribbon

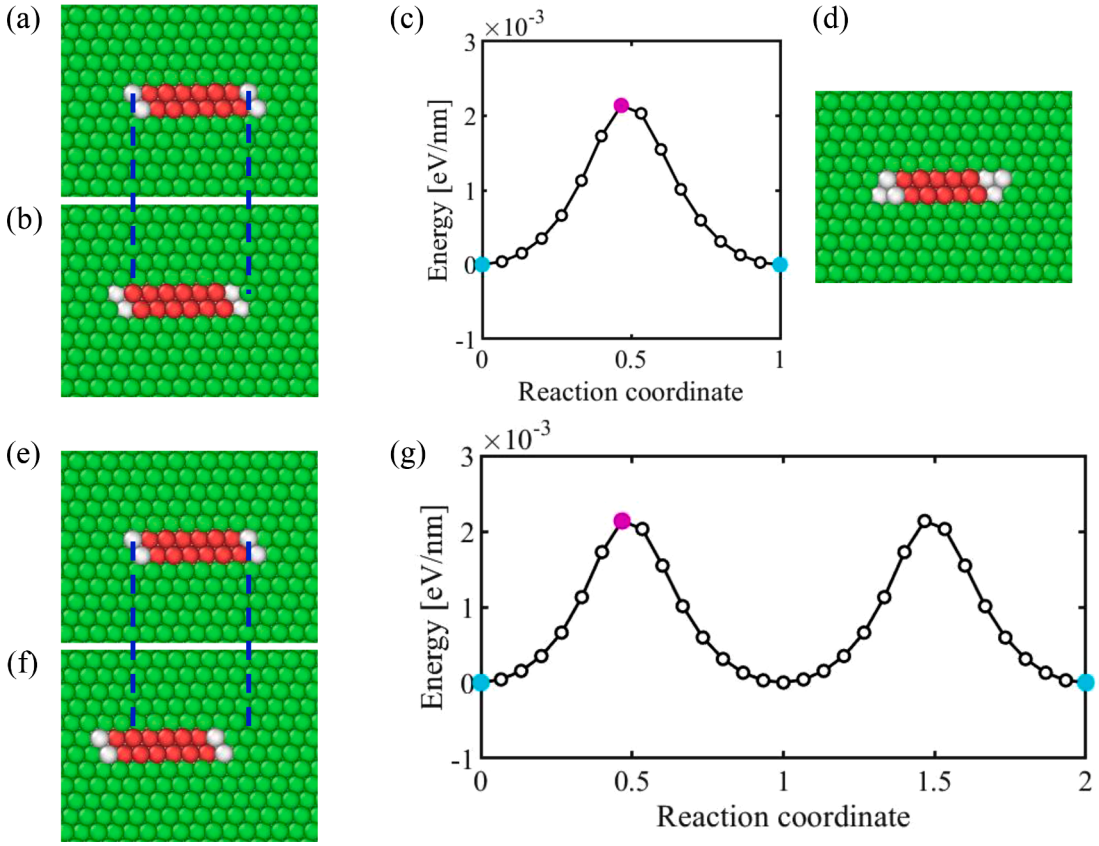

Fig. 2. NEB results of screw dislocation glide without applied loading. Atomic configuration of (a) the initial state and (b) final state from the NEB calculation of screw dislocation glide across a single Peierls barrier. Common neighbor analysis by OVITO is used to color atoms: green atoms indicate the FCC structure, while red and white atoms indicate the dislocation core. The blue dashed lines indicate the glide displacement of the dislocation core from the initial to final state. (c) MEP of screw dislocation glide from (a) to (b). Circles represent energies of replicas. The energies of (a) and (b) are indicated by cyan circles, respectively. (d) Atomic configuration of the saddle-point state along the MEP. The corresponding energy is indicated by a magenta circle in (c). Atomic configuration of (e) the initial state and (f) final state from the NEB calculation of screw glide across two sequential Peierls barriers. (g) MEP of screw dislocation glide from (e) to (f).

in between. Fig. 1b shows the contour of atomic strain ε_{yz} associated with the screw dislocation in Fig. 1a.

We first use the NEB method to calculate the Peierls barrier of screw dislocation glide without loading. The atomic configuration in Fig. 1a is used as the initial state. The magnified dislocation core structure is displayed in Fig 2a. To obtain the final state, we embed a screw dislocation at a position with a quantized glide displacement of 2.16 Å relative to the initial state, as dictated by lattice periodicity along the x//$[11\bar{2}]$ direction. The magnified dislocation core structure of the final state is displayed in Fig. 2b. The blue dashed lines through Fig. 2a and b indicate the quantized glide displacement of the dislocation core from the initial to the final state. A set of sixteen replicas along the initial elastic band is constructed by linear interpolation of atomic positions between the initial and final states. The MEP is converged when the total energy is less than 1×10^{-12} eV for each replica during the NEB calculation.

Fig. 2c shows the MEP of screw dislocation glide across a single Peierls barrier without loading. The energy of the initial state is taken as zero. The reaction coordinate is defined as the normalized path length along the MEP. It represents concerted displacements of all atoms as the screw dislocation glides from the initial to final state, and can be considered approximately as a net glide displacement of the dislocation core from Fig. 2a to b. As discussed earlier, the dislocation line in each replica along the MEP remains straight along the z//$[1\bar{1}0]$ direction. Hence, the energy along all the MEPs in this work is expressed as the energy per unit dislocation length. Fig. 2c shows that the initial and final states have the same energy, as dictated by the translation invariance of dislocation structure in the periodic lattice without applied loading. The maximum, i.e., saddle point, appears in the middle of the MEP, as dictated by the translation invariance as well. The corresponding maximum energy per unit length gives the Peierls barrier of 0.0021 eV/nm without applied loading. Fig. 2d shows the magnified dislocation core structure of the saddle-point state, which exhibits as a right-tilted parallelogram in contrast with a left-tilted parallelogram in the initial and final states (Fig. 2a and b).

We obtain a longer MEP of screw dislocation glide across two sequential Peierls barriers. The initial and final states along this MEP are shown in Fig. 2e and 2f, respectively. Fig. 2g shows the corresponding MEP. As the reaction coordinate is normalized by the path length across a single Peierls barrier, the entire MEP is two times longer than that in Fig. 2c. The two MEP segments associated with two sequential Peierls barriers replicate each other, giving identical Peierls barriers. This result provides direct demonstration of the oscillating dislocation energy in a periodic lattice structure without applied loading.

3. Peierls barrier of screw dislocation glide under shear loading

3.1. ε−NEB results

The strain-controlled NEB (denoted as ε−NEB) method is used to calculate the Peierls barrier of screw dislocation glide under applied loading. For each ε−NEB calculation, it is necessary to apply the same strain for all replicas along the MEP. To obtain the initial state under an applied shear strain, we use the initial state without applied loading as the starting structure, and apply an anti-plane shear strain by imposing an anti-plane displacement to all atoms in the top three layers of the slab, while fixing all atoms in the bottom three layers. The rest of the slab is relaxed by the conjugate gradient method for energy minimization, giving the initial state under an applied shear strain. The same procedure is applied to obtain the final state under the same applied shear strain. Then a set of replicas along an initial elastic band is constructed by linear interpolation of atomic positions between the initial and final states, such that all the intermediate replicas have the same boundary displacement as the initial and final states. As the elastic band is relaxed by the

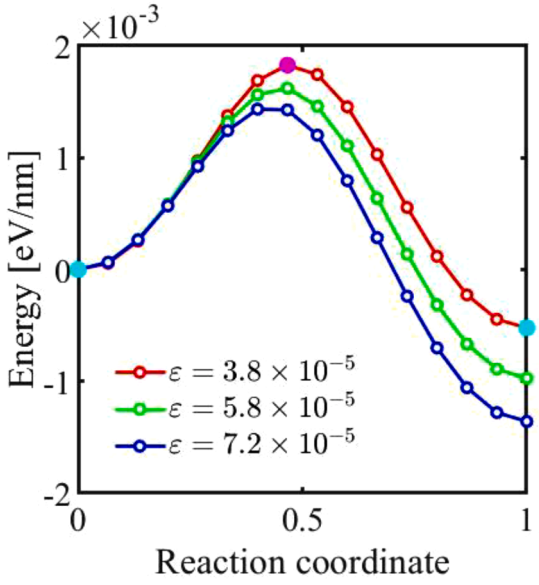

Fig. 3. ε−NEB results showing the MEPs of screw dislocation glide across a single Peierls barrier under three different applied shear strains.

ε−NEB method, boundary atoms in all the replicas are fixed. As such, the same applied shear strain is maintained until a converged MEP is obtained.

Fig. 3 shows the MEPs of screw dislocation glide across a single Peierls barrier under different applied shear strains. Under a low shear strain of 3.8×10^{-5}, the MEP (red curve) is slightly tilted forward, such that the final state has a lower energy than the initial state. The energy of the saddle-point state, i.e., Peierls barrier, is 0.0018 eV/nm, which is a little lower than the Peierls barrier of 0.0021 eV/nm without applied loading. The green and blue curves in Fig. 3 show that the MEP is increasingly tilted as the applied shear strain rises. Correspondingly, both the Peierls barrier and the energy of the final state decrease with increasing shear strain.

The ε−NEB method is also used to determine the MEPs of screw dislocation glide across two sequential Peierls barriers under applied loading. We adopt the same initial state as the NEB calculation for a single Peierls barrier and obtain a new final state where the screw dislocation is moved with a quantized displacement of 4.31 Å relative to the initial state. Fig. 4a shows the corresponding MEPs under different applied shear strains. Fig. 4b–f show the atomic structures in the dislocation core region at local minima and maxima along a representative MEP under an applied shear strain of 7.2×10^{-5} (blue curve in Fig. 4a). The entire MEP consists of two MEP segments, each of which is associated with a Peierls barrier. Incidentally, the first MEP segment is identical to the MEP under the same applied shear strain in Fig. 3. It is seen from Fig. 4a that after the dislocation glides across the first Peierls barrier, the system reaches an intermediate local minimum, which has a lower energy than the initial state. As the dislocation at such a metastable state further glides across the second Peierls barrier to reach the final state, a lower energy is achieved compared to the intermediate local minimum. Since the screw dislocation glides in the slab under a fixed applied shear strain, the plastic shear strain increases and correspondingly the elastic shear strain decreases, thus lowering the shear stress in the slab. As a result, the second MEP segment is subjected to lower shear stresses compared to the first segment, leading to the increased Peierls barrier from the first to the second MEP segment. For example, under an applied shear strain of 7.2×10^{-5}, the second MEP segment gives a higher Peierls barrier of 0.00178 eV/nm than 0.00138 eV/nm from the first MEP segment. These results demonstrate that the Peierls barrier from the ε−NEB calculation is affected by progressive stress relaxation along the MEP. As the system size increases, the stress relaxation effect can become less pronounced. However, when the NEB method is combined with energy calculations based on a computationally intensive quantum mechanical method (Shin and Carter, 2013) or machine-learning potential (MLP) (Mishin, 2021), the model size is usually small. Hence, the Peierls barrier from the ε−NEB calculation should appropriately account for the effect of the system size (see Section 3.3).

3.2. σ−NEB results

The stress-controlled NEB (denoted as σ−NEB) method is used to determine the Peierls barriers of screw dislocation glide under applied loading, which are then compared with the corresponding ε−NEB results. To implement the σ−NEB method in LAMMPS, a fixed force f_z is applied to each atom in the top three layers of the slab, while an opposite force $-f_z$ is applied to each atom in the bottom three layers. Meanwhile, f_x and f_y are kept zero in the boundary layers. The corresponding shear stress is given by $\tau_{yz} = (N \times f_z)/(L_x \times L_z)$, where N is the number of atoms in the top/bottom boundary layer, L_x and L_z are the lengths of the supercell in the x- and z-direction, respectively, and they are kept unchanged during NEB relaxation. This σ−NEB method is different from other stress-controlled NEB methods in the literature (Ghasemi et al., 2019; Huang et al., 2009). For example, all the stress components acting

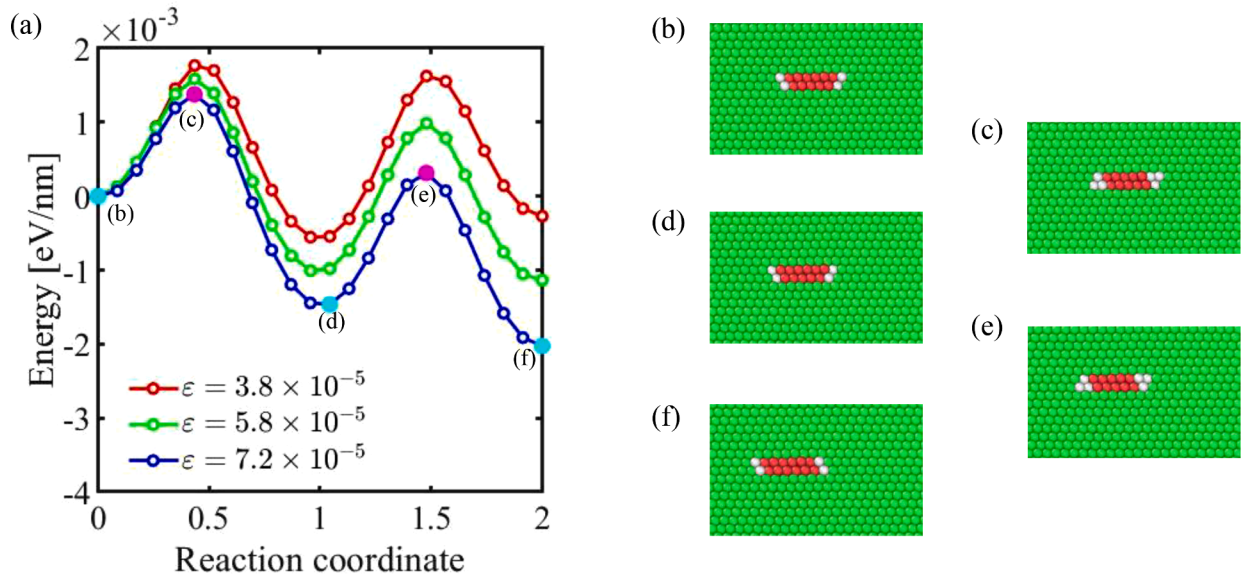

Fig. 4. ε−NEB results of screw dislocation glide across two sequential Peierls barriers under applied loading. (a) MEPs of screw dislocation glide under three different applied shear strains. (b)-(f) Atomic configurations of local minima and saddle points along the MEP under a shear strain of 7.2×10^{-5}, and the corresponding energies are indicated by cyan and magenta circles on the blue curve in (a), respectively.

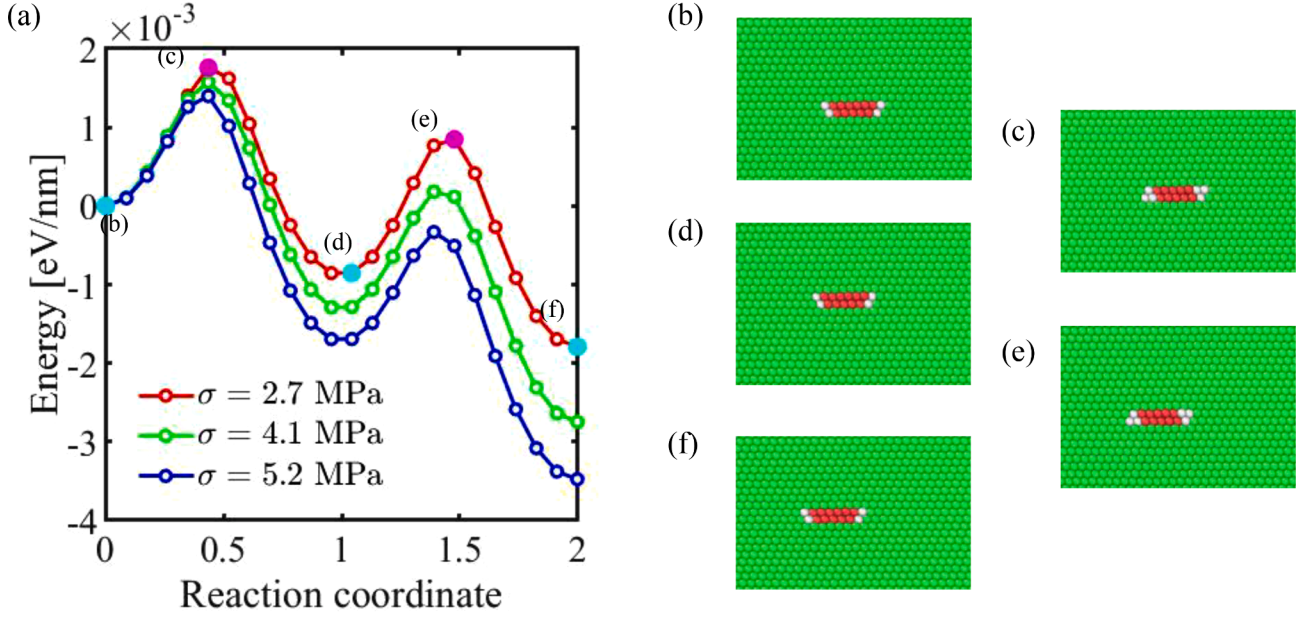

Fig. 5. σ–NEB results of screw dislocation glide across two sequential Peierls barriers under applied loading. (a) MEPs of screw dislocation glide under three different applied shear stresses. (b)–(f) Atomic configurations of local minima and saddle points along the MEP under a shear stress of 2.7 MPa, and the corresponding energies are indicated respectively by cyan and magenta circles on the red curve in (a).

on a supercell can be controlled during NEB relaxation, thus facilitating the study of phase transformation due to the change of supercell geometry (Ghasemi et al., 2019).

Fig. 5a shows the MEPs of screw dislocation glide across two sequential Peierls barriers under different applied shear stresses. Fig. 5b–f display the atomic structures in the dislocation core region at a series of local minima and maxima along a representative MEP under an applied shear stress of 2.7 MPa (red curve in Fig. 5a). The entire MEP consists of two MEP segments, each of which is associated with a Peierls barrier. Since the applied shear stress is constant along the MEP, the two MEP segments exhibit almost identical profiles when the energy of the respective initial state is offset to zero. Hence, the two MEP segments give nearly equal Peierls barriers as well as equal energy decreases from the respective initial to final state. For example, under an applied shear stress of 2.7 MPa, the first and second Peierls barriers are 0.00175 eV/nm and 0.0017 eV/nm, respectively; the energy decreases by 0.00085 and 0.0009 eV/nm from the initial to final state for the respective MEP segment.

To compare the ε−NEB and σ−NEB methods under the same load, we need to convert a shear stress applied to the σ−NEB calculation to an equivalent shear strain applied to the comparative ε−NEB calculation. To this end, we use the shear modulus of the slab of 63 GPa to convert a shear stress to a shear strain, apply this shear strain to the initial state of the ε−NEB calculation, and further adjust it to achieve the target shear stress (as verified from the LAMMPS output). In Fig. 6, we compare the ε−NEB and σ−NEB results in terms of their MEP curves of screw dislocation glide across two sequential Peierls barriers under an applied shear stress of 2.7 MPa. The first MEP segments from the two methods overlap closely with each other, giving almost identical Peierls barriers. However, the second MEP segments are markedly different, giving significantly different Peierls barriers. This difference arises mainly due to the aforementioned stress relaxation effect along the MEP in the ε−NEB calculation. That is, as the screw dislocation glides along the MEP, the applied shear stress is maintained at 2.7 MPa in the σ−NEB calculation, such that the Peierls barriers are identical across the two MEP segments in Fig. 6. In contrast, the shear stress progressively decreases along the MEP in the ε−NEB calculation. The stress decrease is relatively small along the first MEP segment, such that the first Peierls barriers from the ε−NEB and σ−NEB calculations are very close. However, the stress decrease with ε−NEB becomes more substantial along the second MEP segment relative to the applied shear stress at the initial state of the entire MEP. As a result, the second Peierls barrier from the ε−NEB calculation becomes markedly higher than that from the σ−NEB calculation. This comparison indicates that under a prescribed shear stress, the σ−NEB method gives almost constant Peierls barriers across sequential MEP segments, whereas the ε−NEB method yields increasing Peierls barriers across sequential MEP segments. Nonetheless, the ε−NEB method can be used to obtain an approximate estimate of the Peierls barrier from the first MEP segment when the system is sufficiently large (see Section 3.3).

3.3. Size effect

Compared to the ε-NEB method, a major advantage of the σ−NEB method is that the Peierls barrier is almost independent of the system size, so that a small system can be used to save computational cost. For example, Fig. 7a shows the nearly identical σ−NEB results of screw dislocation glide across a Peierls barrier in two systems with the respective in-plane slab sizes of 40 × 40 nm and 20 ×

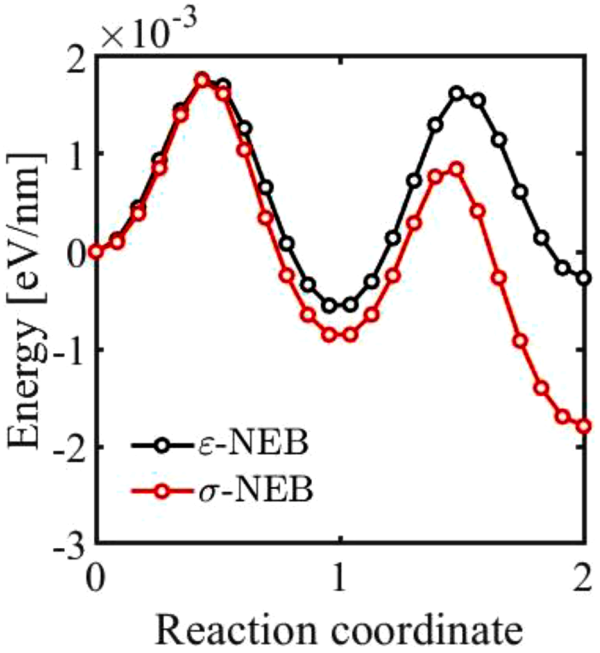

Fig. 6. Comparison between the ε−NEB and σ−NEB methods in terms of the respective MEP of screw dislocation glide across two sequential Peierls barriers under an applied shear stress of 2.7 MPa.

22 nm under an applied shear stress of 2.7 MPa. In contrast, Fig. 7b presents the corresponding ε-NEB results in the two systems, which exhibit a strong dependence on the system size, particularly when the system is small.

The different size effects between the $\sigma-$NEB and ε-NEB methods can be understood as follows. In the $\sigma-$NEB calculation, we move a dislocation from a Peierls valley (i.e., the initial state) to the neighboring one (i.e., the final state). Correspondingly, both the displacement and stress fields of this dislocation are translated. As a result, the structures of the initial and final states maintain the translation invariance, such that the minimum energy path and associated energy barrier are almost insensitive to the system size (as shown in Fig. 7a). In contrast, as we move the dislocation in the strain-controlled NEB calculation, the atom positions in the top and boundary layers in the final state are the same as the initial state. The constraining effect of the fixed boundary layers causes a change of stress distribution around the moved dislocation in the final state. This constraining effect increases with decreasing system size. Therefore, the minimum energy path and associated energy barrier are more sensitive to the system size (as shown in Fig. 7b). Hence, the $\sigma-$NEB method is better suited for the atomistic determination of Peierls barriers when energy calculations rely on a computationally intensive quantum mechanical method (Shin and Carter, 2013) or MLP (Mishin, 2021), for example.

3.4. Peierls stress

The Peierls stress is the critical resolved shear stress corresponding to the vanishing Peierls barrier, leading to instantaneous dislocation glide without the aid of thermal fluctuations. To determine the Peierls stress of screw dislocation glide, we use the $\sigma-$NEB method to calculate the Peierls barriers for a wide range of applied shear stresses, with the same simulation setup as those for the first MEP segment in Fig. 5a. Fig. 8 shows the $\sigma-$NEB results of decreasing Peierls barriers (blue circles) with increasing shear stress. These data points are fitted by a nonlinear function (Zhu et al., 2008)

$$Q(\tau) = A\left(1 - \frac{\tau}{\tau_{\text{ath}}}\right)^{\alpha} \tag{2}$$

where Q is the Peierls barrier, τ is the applied shear stress, τ_{ath} is the Peierls stress (i.e., the intercept with the stress axis), A is the energy barrier at $\tau = 0$, and α is the nonlinear profiling parameter. The least squares fitting gives $\tau_{\text{ath}} = 21$ MPa, $\alpha = 1.6$, and $A = 0.0021$ eV/nm, the last of which matches the direct NEB result without applied loading in Section 2.

3.5. Free-end $\varepsilon-$NEB and $\sigma-$NEB results

The free-end NEB method (Zhu et al., 2007, 2008) has been previously developed to enable the efficient determination of a long MEP that is highly tilted by loading. Compared to the conventional NEB method, the final state for the free-end NEB method is not required to be a local minimum, and it is allowed to freely move at a prescribed energy level as the elastic band is relaxed. As a result, a short elastic band can be used to improve the computational efficiency. In this work, we use the free-end $\varepsilon-$NEB and $\sigma-$NEB methods to determine the MEP of screw dislocation glide through LAMMPS. For example, Fig. 9a shows the fixed-end $\varepsilon-$NEB result of an MEP of screw dislocation glide under a high shear strain of 7.2×10^{-5} (corresponding to a shear stress of 5.2 MPa). In this calculation, the MEP connects the initial and final states of local energy minimum, and 24 replicas (circles) are used to represent the entire MEP. Since the MEP is highly tilted by applied loading, the saddle-point state becomes close to the initial state. To capture such a saddle-point state, it

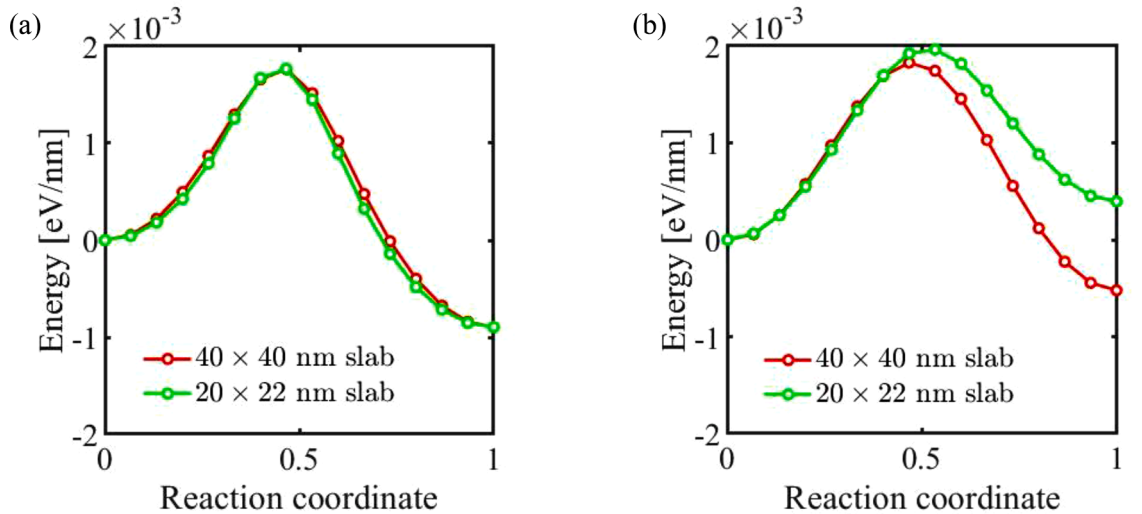

Fig. 7. Sample size effects on NEB results. (a) Comparison of $\sigma-$NEB results of screw dislocation glide across two sequential Peierls barriers under an applied shear stress of 2.7 MPa for a larger slab of 40 × 40 nm and a smaller one of 20 × 22 nm, respectively. (b) Same as (a) except for comparison of $\varepsilon-$NEB results.

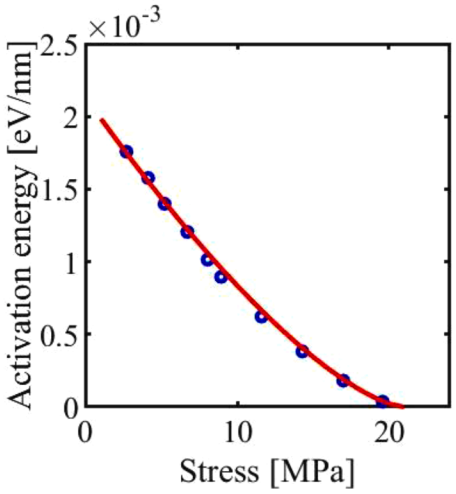

Fig. 8. Peierls barrier versus resolved shear stress from $\sigma-$NEB calculations of screw dislocation glide across a Peierls barrier. Blue circles represent calculated Peierls barriers at different shear stresses, and the red solid line is the fitting curve according to Eq. (2).

is not necessary to map out the whole elastic band beyond the saddle-point state. Hence, we choose a replica (marked by the blue dot in Fig. 9a) that is beyond the saddle point and has an energy close to the initial state, and use this replica as the initial free-end state. In the free-end $\varepsilon-$NEB calculation, 16 replicas are used to represent the elastic band and the free-end state is kept at the same energy level as the initial state. Fig. 9b shows the MEP between the initial and free-end states with less replicas but a similar replica density compared to the MEP from the fixed-end NEB result in Fig. 9a. It is seen that the saddle-point state and associated energy barrier closely match those from the fixed-end $\varepsilon-$NEB calculation.

Similarly, Fig. 9c shows the fixed-end $\sigma-$NEB result of an MEP of screw dislocation glide under a high shear stress of 5.2 MPa. In this calculation, the MEP connects the initial and final states of local energy minimum, and 24 replicas (circles) are used to represent the entire MEP. In the free-end $\sigma-$NEB calculation, we choose a replica (marked by the blue dot in Fig. 9c) that is beyond the saddle point and has an energy close to the initial state, and use this replica as the initial free-end state. In the free-end $\sigma-$NEB calculation, 16 replicas are used to represent the elastic band and the free-end state is kept at same energy level as the initial state. Fig. 9d shows the MEP between the initial and free-end states. The saddle-point state and associated energy barrier closely match those from the fixed-end $\sigma-$NEB calculation. The above results demonstrate the efficiency of the free-end $\varepsilon-$NEB and free-end $\sigma-$NEB methods relative to their fixed-end counterparts.

4. Peierls barrier of edge dislocation glide

We use the $\sigma-$NEB method to determine the Peierls barriers of edge dislocation glide, which are compared with those of screw dislocation glide. We employ the setup similar to that for the $\sigma-$NEB calculation of screw dislocation glide, except that the slab is oriented in the x//$[\bar{1}10]$, y//$[111]$, and z//$[11\bar{2}]$ directions and subjected to an applied in-plane shear stress. To embed an edge dislocation in the slab, atoms in an upper half $(\bar{1}10)$ plane (parallel to y-z plane) are removed and then the slab is relaxed by the conjugate gradient method for energy minimization. The resulting local energy minimum is taken as the initial state. Similarly, the final state is obtained by removing atoms in a neighboring half $(\bar{1}10)$ plane.

Fig. 10a shows the MEP of edge dislocation glide across a Peierls barrier without applied loading. Fig. 10b–d displays the atomic structure in the dislocation core region at the initial, saddle point and final states along the MEP, respectively. It is seen from Fig. 10a that the Peierls barrier without applied loading is 0.000055 eV/nm, which is much lower than the Peierls barrier of 0.0021 eV/nm for screw dislocation glide without applied loading. This result indicates that the edge dislocation is more mobile than the screw dislocation in pure Ni, which is consistent with a general trend from experiments regarding the higher mobility of edge than screw dislocations in FCC metals (Adams and Cottrell, 1955) in the thermally-assisted flow regime.

To study the loading effect on edge dislocation glide, we use the $\sigma-$NEB method to determine the MEPs across two sequential Peierls barriers under different shear stresses. As shown in Fig. 11, the higher the applied shear stress, the more the MEP is tilted. Since the applied shear stress is constant along each MEP, the two MEP segments give nearly equal Peierls barriers as well as equal energy decreases from the respective initial to final state. These results are similar to the stress effect on the MEPs for screw dislocation glide in Fig. 5a. Note that these shear stresses, however, are very low compared to those for the case of a screw dislocation, consistent with the relative reduction of the Peierls barrier for the edge dislocation relative to the screw dislocation.

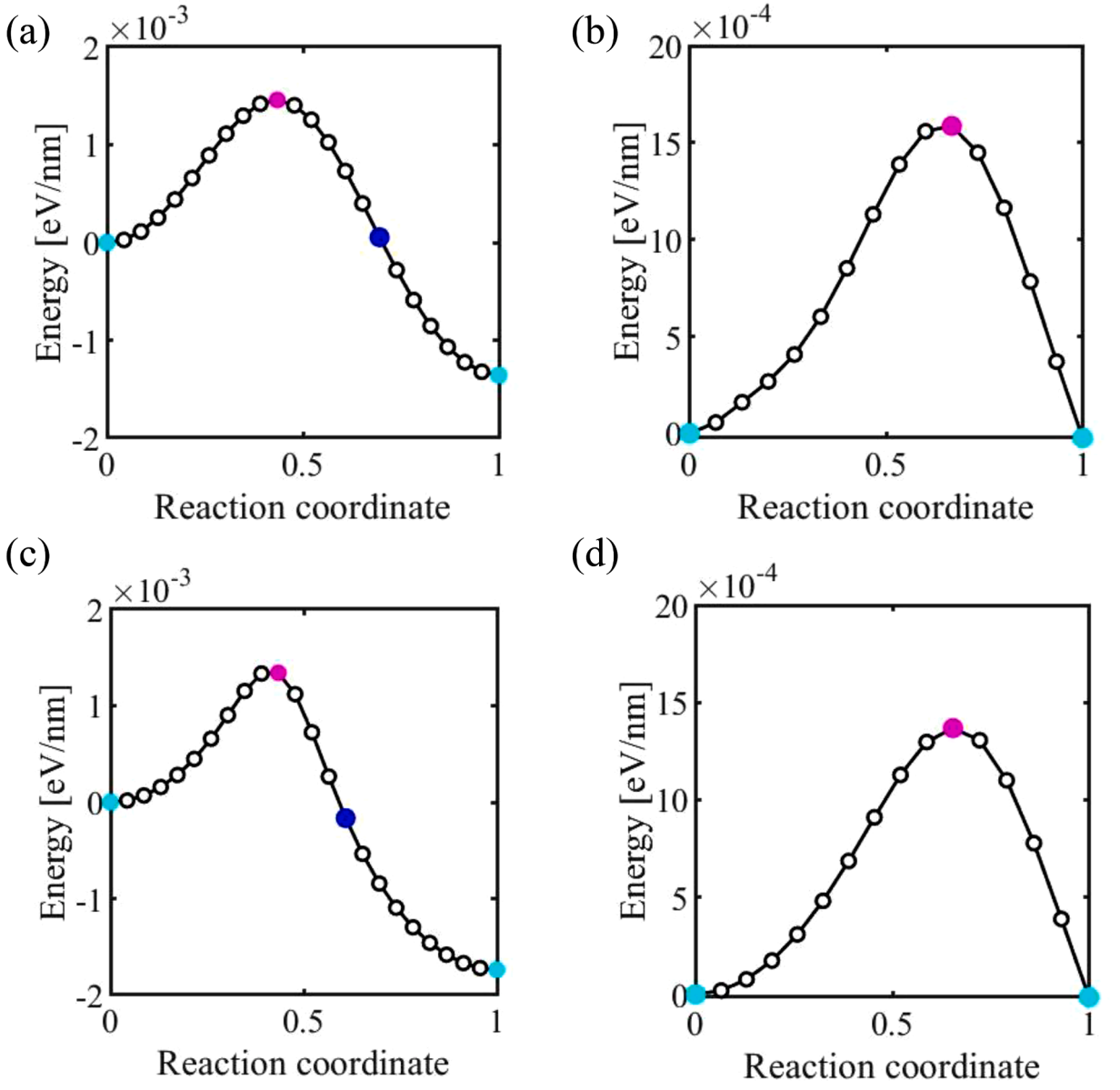

Fig. 9. Free-end NEB results for screw dislocation glide under high shear loading. (a) A fixed-end ε−NEB result showing the MEP of screw dislocation glide across a single Peierls barrier under a shear strain of 7.2×10^{-5} (corresponding to a shear stress of 5.2 MPa). (b) Same as (a) except that the free-end ε−NEB method is used. (c) A fixed-end σ−NEB result showing the MEP of screw dislocation glide across a single Peierls barrier under a shear stress of 5.2 MPa. (d) Same as (c) except that the free-end σ−NEB method.

5. Discussion

5.1. Peach-Koehler force

The Peach-Koehler force represents the energetic force exerted on a dislocation under an applied shear stress on the slip plane, and it is widely used as the driving force on dislocation motion. The general formula of the Peach-Koehler force has been derived for a three-dimensional dislocation loop (Peach and Koehler, 1950). Here we consider the application of this formula to a straight dislocation segment, such that the Peach-Koehler force per unit length takes a simple analytic form of $\tau \cdot b$, where τ is the revolved shear stress and b is the magnitude of the Burgers vector. The Peach-Koehler force is used to validate the atomistically calculated energy

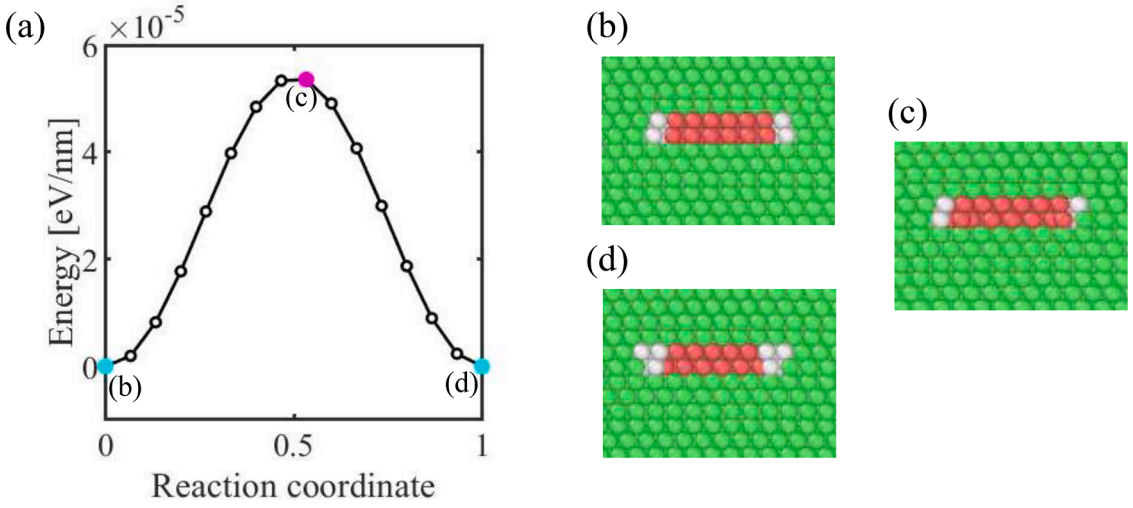

Fig. 10. σ−NEB result of edge dislocation glide without applied loading. (a) MEP of edge dislocation glide across a single Peierls barrier without applied loading. Atomic configurations of (b) initial, (c) saddle-point and (d) final states along the MEP, and their corresponding energies are indicated as cyan, magenta and cyan circles in (a), respectively.

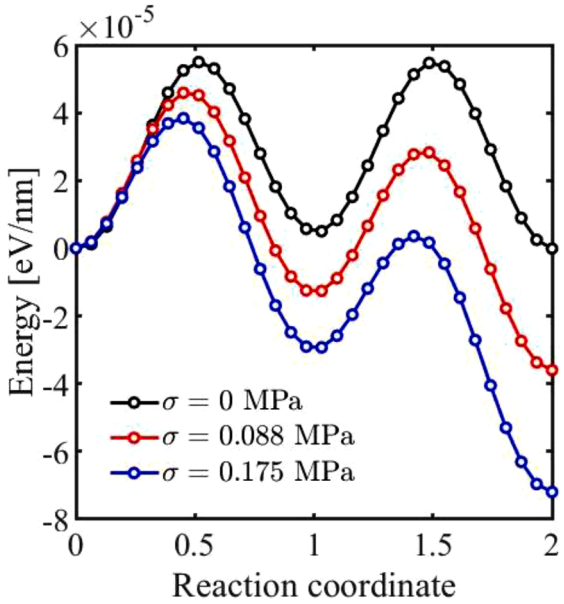

Fig. 11. σ−NEB results showing the MEPs of edge dislocation glide across two sequential Peierls barriers under three different applied shear stresses.

decrease ΔE from the initial to final state on an MEP of screw dislocation glide under an applied shear stress τ. In the corresponding NEB calculation, we denote L as the length of the dislocation segment and Δx as the dislocation displacement from the initial to final state. Then the atomistically calculated ΔE should satisfy the relation of $\Delta E = \tau \cdot b \cdot \Delta x \cdot L$, where the right-hand side term is the work done by the Peach-Koehler force upon a dislocation displacement of Δx.

Fig. 12 shows the σ−NEB result of an MEP of screw dislocation glide across four sequential Peierls barriers. Correspondingly, Δx should be four times the unit glide displacement between Fig. 2a and b. From the MEP in Fig. 12, we obtain the energy decrease ΔE from the initial to final state as 0.00358 eV/nm. On the other hand, we calculate the corresponding energy decrease as $\tau \cdot b \cdot \Delta x \cdot L =$ 0.00358 eV/nm, with $\tau = 2.7$ MPa, $b =$ 2.49 Å, $\Delta x = 8.62$ Å and $L = 1$ nm (normalized as the unit dislocation length). The identical values of energy decrease between the two results provide direct validation of the atomistically calculated energy decrease ΔE from the initial and final state on an MEP of screw dislocation glide under the applied shear stress τ. We note that the Peach-Koehler

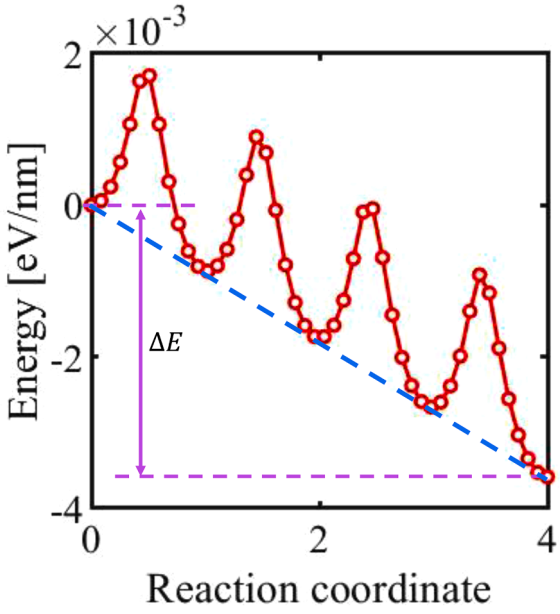

Fig. 12. σ−NEB result showing the MEP of screw dislocation glide across four sequential Peierls barriers under an applied shear stress of 2.7 MPa. ΔE is energy decrease from the initial to final states along the MEP. The Peach-Koehler force corresponds to the slope of the envelope curve (blue dashed line) connecting local minima along the MEP.

Table 1
FCC Ni mechanical properties predicted with DFT and MLP.

Property	DFT	MLP
C_{11} (GPa)	267	244
C_{12} (GPa)	155	155
C_{44} (GPa)	139	126
Bulk modulus (GPa)	193	184
Shear modulus (GPa)	96	83
Poisson's ratio	0.29	0.30
Stacking fault energy (mJ/m^2)	127	138

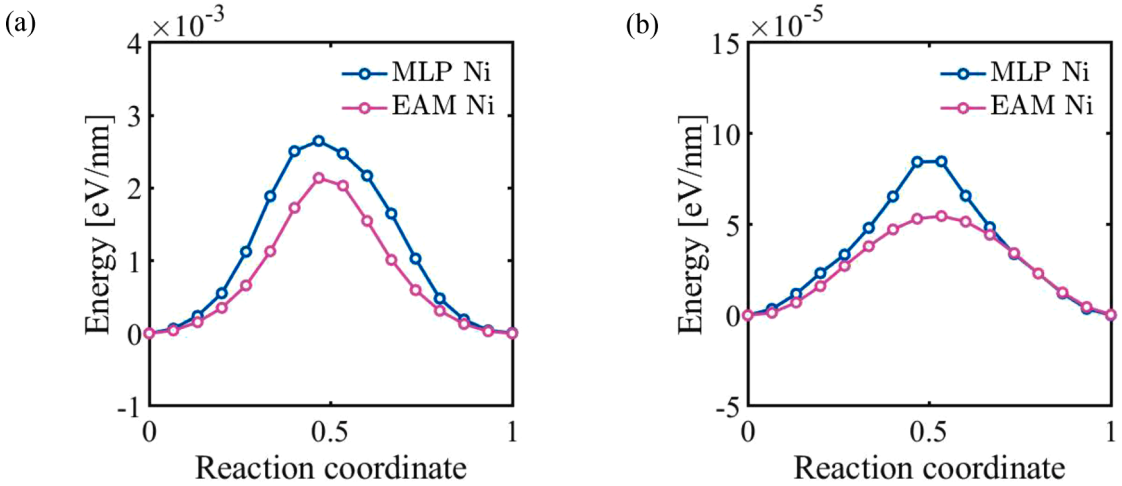

Fig. 13. Comparison of NEB results between EAM Ni and MLP Ni potentials. (a) MEPs of screw dislocation glide across a Peierls barrier. (b) Same as (a) except for edge dislocation glide.

force is the energetic force representing the rate of energy decrease as the dislocation moves from the initial to final state of local energy minimum. Hence, the Peach-Koehler force corresponds to the slope of the envelope curve (blue dashed line) connecting local minima along the MEP of dislocation glide in Fig. 12.

5.2. Peierls barrier from MLP

MLPs can predict the energy and atomic force with high accuracy close to quantum mechanical methods while enabling orders of magnitude faster atomistic simulations (Mishin, 2021). A pure-Ni MLP belonging to the class of spectral neighbor analysis potential (SNAP) (Thompson et al., 2015) was developed by Materials Design Inc. and Naval Nuclear Laboratory. A large data set from first-principles density functional theory (DFT) calculations was used to train the MLP, which includes but is not limited to self-interstitial energy, vacancy energy, elastic constants, and stacking fault energy. The MLP reproduces DFT energy of Ni with generally less than 0.004 eV/atom for all structures in the training set. Table 1 compares mechanical properties from the SNAP and DFT calculations of FCC Ni.

Here, we use the MLP Ni to calculate the Peierls barriers of screw and edge dislocation glide in Ni, which are compared with the results based on the EAM potential of Ni (denoted as EAM Ni) used in this work (Angelo et al., 1995). Fig. 13a shows the MEPs of screw dislocation glide across a single Peierls barrier from the two potentials. The Peierls energy barrier is 0.002 eV/nm from EAM Ni and 0.0026 eV/nm from MLP Ni, respectively. In addition, Fig. 13b shows the MEPs of edge dislocation glide across a single Peierls barrier from the two potentials. The Peierls barrier is 0.00006 eV/nm from EAM Ni and 0.00009 eV/nm from MLP Ni. These results indicate that EAM Ni and MLP Ni give close Peierls barriers, thus lending support to the accuracy of the NEB results based on EAM Ni.

6. Conclusions

We have performed NEB calculations of the Peierls barriers of screw and edge dislocation glide in FCC Ni. The MEPs and associated Peierls barriers are determined for different applied loads, boundary conditions and system sizes. The main results are summarized as follows.

- In the absence of applied loading, the Peierls barriers are shown to be low for both screw and edge dislocations in FCC Ni, but the screw type has a higher Peierls barrier than the edge type.
- Both the strain- and stress-controlled NEB methods are used to determine Peierls barriers across sequential Peierls barriers under applied shear stress, showing the decreased Peierls barrier with increasing applied shear stress. The two methods give close values of the first Peierls barrier when the system is sufficiently large. However, due to stress relaxation with dislocation glide in the strain-controlled NEB calculation, the sequential Peierls barriers are not constant in this case. In contrast, the stress-controlled NEB calculation gives constant Peierls barriers for different system sizes as well as across sequential Peierls barriers. These results demonstrate that the stress-controlled NEB method enables an efficient atomistic determination of Peierls barriers of screw and edge dislocation glide using small samples for FCC crystals. Hence, the stress-controlled NEB method is better suited for the atomistic determination of Peierls barriers when energy calculations rely on a computationally intensive quantum mechanical method or MLP.
- The stress-controlled NEB method is used to accurately determine the Peierls stress by fitting the Peierls barriers to a nonlinear function under a broad range of applied shear stresses.
- The strain- and stress-controlled free-end NEB methods are shown to be more computationally efficient than the fixed-end NEB methods, particularly when dealing with long MEPs tilted by high loads.
- The Peach-Koehler force is used to validate the atomistically calculated energy decrease from the initial to final states on an MEP of dislocation glide under an applied shear stress. This result also demonstrates the atomistic manifestation of the Peach-Koehler force as the energetic force driving dislocation motion, which corresponds to the slope of the envelope curve connecting local minima along the MEP of dislocation glide.
- The MLP-based NEB results of the Peierls barriers for screw and edge dislocations in Ni indicate the accuracy of the EAM-based NEB results in this work.

Altogether, our work demonstrates the robust and efficient quantification of Peierls barriers to dislocation glide in a representative FCC metal, and it lays a solid foundation for the atomistic determination of Peierls barriers in compositionally complex alloys with the FCC structure in the future.

CRediT authorship contribution statement

Yipin Si: Investigation, Validation, Formal analysis, Visualization, Methodology, Writing – original draft, Writing – review & editing. **Yin Zhang:** Investigation, Methodology. **Dengke Chen:** Investigation, Methodology. **Jonathan L. Wormald:** Supervision, Methodology, Writing – review & editing. **Benjamin S. Anglin:** Supervision, Methodology, Writing – review & editing. **David L. McDowell:** Funding acquisition, Supervision, Writing – review & editing. **Ting Zhu:** Conceptualization, Methodology, Funding acquisition, Supervision, Writing – review & editing.

Declaration of Competing Interest

The authors declare that they have no known competing financial interests or personal relationships that could have appeared to influence the work reported in this paper.

Acknowledgments

The authors are grateful for the support from the Naval Nuclear Laboratory, operated by Fluor Marine Propulsion, LLC for the US Naval Reactors Program. The submitted manuscript has been authored by contractors of the US Government under contract No. DOE-89233018CNR000004. Accordingly, the US Government retains a non-exclusive, royalty-free license to publish or reproduce the published form of this contribution, or allow others to do so, for US Government purposes.

References

Angelo, J.E., Moody, N.R., Baskes, M.I., 1995. Trapping of hydrogen to lattice defects in nickel. Model. Simul. Mater. Sci. Eng. 3, 289.
Bai, Z., Fan, Y., 2018. Abnormal strain rate sensitivity driven by a unit dislocation-obstacle interaction in bcc Fe. Phys. Rev. Lett. 120, 125504.
Bulatov, V.V., Richmond, O., Glazov, M.V., 1999. An atomistic dislocation mechanism of pressure-dependent plastic flow in aluminum. Acta Mater. 47, 3507–3514.
Cai, W., Bulatov, V.V., Chang, J.P., Li, J., Yip, S., Nabarro, F.R.N., Hirth, J.P., 2004. Dislocation core effects on mobility. Dislocations in Solids. Elsevier, Amsterdam, pp. 1–80.
Chen, D., Costello, L.L., Geller, C.B., Zhu, T., McDowell, D.L., 2019. Atomistic modeling of dislocation cross-slip in nickel using free-end nudged elastic band method. Acta Mater. 168, 436–447.
Cottrell, A.H., 1953. Dislocations and Plastic Flow in Crystals. Oxford University Press, London.
Ding, Q., Zhang, Y., Chen, X., Fu, X., Chen, D., Chen, S., Gu, L., Wei, F., Bei, H., Gao, Y., Wen, M., Li, J., Zhang, Z., Zhu, T., Ritchie, R.O., Yu, Q., 2019. Tuning element distribution, structure and properties by composition in high-entropy alloys. Nature 574, 223–227.
George, E.P., Curtin, W.A., Tasan, C.C., 2020. High entropy alloys: a focused review of mechanical properties and deformation mechanisms. Acta Mater. 188, 435–474.
Ghasemi, A., Xiao, P., Gao, W., 2019. Nudged elastic band method for solid-solid transition under finite deformation. J. Chem. Phys. 151, 054110.
Huang, S., Zhang, S.L., Belytschko, T., Terdalkar, S.S., Zhu, T., 2009. Mechanics of nanocrack: fracture, dislocation emission, and amorphization. J. Mech. Phys. Solids 57, 840–850.
Jonsson, H., G. Mills, K.W. Jacobsen, 1998. Nudged elastic band method for finding minimum energy paths of transitions In B.J. Berne, G. Ciccotti, and D.F. Coker, eds, Classical and Quantum Dynamics in Condensed Phase Simulations, 385–404.
Li, Q.J., Sheng, H., Ma, E., 2019. Strengthening in multi-principal element alloys with local-chemical-order roughened dislocation pathways. Nat. Commun. 10, 3563.
Lu, G., Kioussis, N., Bulatov, V.V., Kaxiras, E., 2000. The Peierls-Nabarro model revisited. Philos. Mag. Lett. 80, 675–682.
Mishin, Y., 2021. Machine-learning interatomic potentials for materials science. Acta Mater. 214, 116980.
Nabarro, F.R.N., 1947. Dislocations in a simple cubic lattice. Proc. Phys. Soc. 59, 256–272.
Nabarro, F.R.N., 1997. Theoretical and experimental estimates of the Peierls stress. Philos. Mag. A 75, 703–711.
Narayanan, S., McDowell, D.L., Zhu, T., 2014. Crystal plasticity model for BCC iron atomistically informed by kinetics of correlated kinkpair nucleation on screw dislocation. J. Mech. Phys. Solids 65, 54–68.
Peach, M., Koehler, J., 1950. The forces exerted on dislocations and the stress fields produced by them. Phys. Rev. 80, 436.
Peierls, R., 1940. The size of a dislocation. Proc. Phys. Soc. 52, 34–37.
Phillips, R., 2001. Crystals, Defects and Microstructures: Modeling Across Scales. Cambridge University Press, Cambridge, UK.
Ren, J., Zhang, Y., Zhao, D., Chen, Y., Guan, S., Liu, Y., Liu, L., Peng, S., Kong, F., Poplawsky, J.D., Gao, G., Voisin, T., An, K., Wang, Y.M., Xie, K.Y., Zhu, T., Chen, W., 2022. Strong yet ductile nanolamellar high-entropy alloys by additive manufacturing. Nature 608, 62–68.
Rodney, D., Proville, L., 2009. Stress-dependent Peierls potential: influence on kink-pair activation. Phys. Rev. B 79, 094108.
Rodney, D., Ventelon, L., Clouet, E., Pizzagalli, L., Willaime, F., 2017. Ab initio modeling of dislocation core properties in metals and semiconductors. Acta Mater. 124, 633–659.
Schoeck, G., 1999. Peierls energy of dislocations: a critical assessment. Phys. Rev. Lett. 82, 2310–2313.
Shin, I., Carter, E.A., 2013. Possible origin of the discrepancy in Peierls stresses of fcc metals: first-principles simulations of dislocation mobility in aluminum. Phys. Rev. B 88, 064106.
Stukowski, A., 2010. Visualization and analysis of atomistic simulation data with OVITO–the Open Visualization Tool. Modelling Simul. Mater. Sci. Eng. 18, 015012.
Szelestey, P., Patriarca, M., Kaski, K., 2003. Computational study of core structure and Peierls stress of dissociated dislocations in nickel. Model. Simul. Mater. Sci. Eng. 11, 883–895.
Thompson, A.P., Aktulga, H.M., Berger, R., Bolintineanu, D.S., Brown, W.M., Crozier, P.S., Veld, P.J., Kohlmeyer, A., Moore, S.G., Nguyen, T.D., Shan, R., Stevens, M. J., Tranchida, J., Trott, C., Plimpton, S.J., 2022. LAMMPS - a flexible simulation tool for particle-based materials modeling at the atomic, meso, and continuum scales. Comput. Phys. Commun. 271, 108171.
Thompson, A.P., Swiler, L.P., Trott, C.R., Foiles, S.M., Tucker, G.J., 2015. Spectral neighbor analysis method for automated generation of quantum-accurate interatomic potentials. J. Comput. Phys. 285, 316–330.
Vineyard, G.H., 1957. Frequency factors and isotope effects in solid state rate processes. J. Phys. Chem. Solids 3, 121–127.
Wang, R., Wang, S., Wu, X., 2011. Edge dislocation core structures in FCC metals determined from ab initio calculations combined with the improved Peierls–Nabarro equation. Phys. Scr. 83, 045604.
Wang, X., Maresca, F., Cao, P., 2022. The hierarchical energy landscape of screw dislocation motion in refractory high-entropy alloys. Acta Mater. 234, 118022.
Wu, Z., Curtin, W.A., 2015. The origins of high hardening and low ductility in magnesium. Nature 526, 62–67.
Zhang, Y., Ding, K., Stangebye, S., Chen, D., Kacher, J., Pierron, O., Zhu, T., 2022. Atomistic modeling of surface and grain boundary dislocation nucleation in FCC metals. Acta Mater. 237, 118155.
Zhu, T., Li, J., Samanta, A., Kim Hyoung, G., Suresh, S., 2007. Interfacial plasticity governs strain rate sensitivity and ductility in nanostructured metals. Proc. Natl. Acad. Sci. 104, 3031–3036.
Zhu, T., Li, J., Samanta, A., Leach, A., Gall, K., 2008. Temperature and strain-rate dependence of surface dislocation nucleation. Phys. Rev. Lett. 100, 025502.
Zhu, T., Li, J., Yip, S., 2013. Atomistic reaction pathway sampling: the nudged elastic band method and nanomechanics applications. Nano Cell Mech.: Fundam. Front. 311–338.